

# The contribution of the Warm-Hot Intergalactic Medium to the CMB anisotropies via the Sunyaev-Zeldovich effect

I. F. Suarez-Velásquez<sup>1\*</sup>, J. P. Mücke<sup>1</sup> and F. Atrio-Barandela<sup>2</sup>

<sup>1</sup>*Leibniz-Institut für Astrophysik Potsdam, An der Sternwarte 16, 14482, Potsdam, Germany*

<sup>2</sup>*Física Teórica, Universidad de Salamanca, Plaza de la Merced s/n, 37008 Salamanca, Spain*

Accepted . Received ; in original form 2012

## ABSTRACT

Cosmological hydrodynamical simulations predict that a large fraction of all baryons reside within mildly non-linear structures with temperatures in the range  $10^5 - 10^7$  K. As the gas is highly ionized, it could be detected by the temperature anisotropies generated on the Cosmic Microwave Background radiation. We refine our previous estimates of the thermal Sunyaev-Zeldovich effect by introducing a non-polytropic equation of state to model the temperature distribution of the shock heated gas derived from temperature-density phase diagrams of different hydrodynamical simulations. Depending on the specific model, the Comptonization parameter varies in the range  $10^{-7} \leq y_c \leq 2 \times 10^{-6}$ , compatible with the FIRAS upper limit. This amplitude is in agreement with a simple toy model constructed to estimate the average effect induced by filaments of ionized gas. Using the log-normal probability density function we calculate the correlation function and the power spectrum of the temperature anisotropies generated by the WHIM filaments. For a wide range of the parameter space, the maximum amplitude of the radiation power spectrum is  $(\ell + 1)\ell C_\ell / 2\pi = 0.7 - 70 (\mu K)^2$  at  $\ell \approx 200 - 500$ . This amplitude scales with baryon density, Hubble constant and the amplitude of the matter power spectrum  $\sigma_8$  as  $[(\ell + 1)\ell C_\ell]_{\max} / 2\pi \propto \sigma_8^{2.6} (\Omega_b h)^2$ . Since the thermal Sunyaev-Zeldovich effect has a specific frequency dependence, we analyze the possibility of detecting this component with the forthcoming Planck data.

**Key words:** Missing baryons, WHIM, Sunyaev-Zeldovich

## 1 INTRODUCTION

The distribution of baryons in the local Universe is one of the main problems of modern Cosmology. The highly ionized intergalactic gas, that evolved from the initial density perturbations into a complex network of mildly non-linear structures in the redshift interval  $2 < z < 6$  (Rauch 1998; Stocke et al. 2004), could contain most of the baryons in the universe (Rauch et al. 1997; Schaye 2001; Richter et al. 2006). At redshifts  $z > 2$  most baryons are found in the Ly $\alpha$  systems detected through absorption lines in the spectra of distant quasars. With cosmic evolution, the baryon fraction in these structures decreases as more matter is concentrated within compact virialized objects. At low redshifts, the Ly $\alpha$  systems are filaments with low HI column densities containing  $\sim 30\%$  of all baryons (Stocke et al. 2004), while the material in stars and galaxies contains about 10% of all baryons. An extra 5% could be in the form of Circumgalactic Medium around galaxies (Gupta et al. 2012). More importantly, at  $z \sim 0$  about 50% of all cosmic baryons have not yet

been identified (Fukugita & Peebles 2004; Shull et al. 2011). Hydrodynamical simulations predicted that baryons could be in the form of shock-heated intergalactic gas in mildly-nonlinear structures with temperatures  $10^5 - 10^7$  K, called Warm-Hot Intergalactic Medium (WHIM). The baryon fraction in this medium could be as large as 40%-50% in the local Universe (Cen & Ostriker 1999; Davé et al. 1999, 2001; Danforth & Shull 2008; Prochaska & Tumlinson 2008; Smith et al. 2011) containing the bulk, if not all, the unidentified baryons.

The observational effort has concentrated in searching for the WHIM X-ray signature both in emission and in absorption. Sołtan (2006) looked for the extended soft X-ray emission around field galaxies but his task was complicated by the need to subtract all systematic effects that could mimic the diffuse signal. More recently, the effort has been concentrated in searching for absorption lines due to highly ionized heavy elements from the far-ultraviolet to the soft X-ray (see Shull et al. 2011, for a review) with partial success. For example, Dietrich et al. (2012) have recently reported the detection of a large-scale filament between two clusters of galaxies.

\* E-mail: isuarez@aip.de; jpmuecket@aip.de; atrio@usal.es

While absorption lines will identify individual systems, complementary techniques are needed to study the overall properties of the WHIM. To this purpose, Atrio-Barandela & Mückel (2006) and Atrio-Barandela et al. (2008) suggested that the WHIM distribution would generate temperature anisotropies on the Cosmic Microwave Background (CMB) due to the thermal (TSZ) and kinematic (KSZ) Sunyaev-Zeldovich effect (Sunyaev & Zeldovich 1972, 1980), opening a new observational window to study the gas distribution at low redshifts (Génova-Santos et al. 2009). Hallman et al. (2007) found that about a third of the SZ flux would be generated by unbound gas, but their estimated amplitude was lower than the prediction of our model. Our computation assumed that the weakly non-linear matter distribution was described by a log-normal probability distribution function PDF (Coles & Jones 1991; Choudhury et al. 2001) and the gas followed a polytropic equation of state. While the IGM at redshifts  $z > 2$  behaves like a polytrope, at low redshifts the polytropic equation of state is not longer valid since the gas is heated mostly by shocks to temperatures about  $10^5 K < T < 10^7 K$  at density contrasts  $\delta < 100$ . In the regions where the gas is shock-heated, small-scale density perturbations can be neglected due to the high pressure gradients (Klar & Mückel 2010), simplifying the treatment. In this paper we shall improve our previous calculations by using equations of state derived from hydrodynamical simulations to provide a more physical description of the WHIM. Briefly, in section 2 we estimate the order of magnitude contribution of a population of WHIM filaments to the Comptonization parameter based on a crude geometrical model; in section 3 we describe our log-normal model and we detail the differences with our previous treatments; in section 4 we compute the CMB Comptonization parameter due to the WHIM and in section 5 the correlation function and angular power spectrum; in section 6 we present our results and, finally, in section 7 we summarize our conclusions.

## 2 ESTIMATE OF THE MEAN COMPTONIZATION PARAMETER DUE TO THE WHIM

The temperature anisotropies due to the inverse Compton scattering of CMB photons by the free electrons have only been measured for clusters of galaxies. There are two contributions: the thermal component (TSZ) due to the motion of the electrons in the potential wells and the kinematic component (KSZ) due to the motion of the cluster as a whole. The induced temperature anisotropies are

$$\left(\frac{\delta T}{T_0}\right)_{\text{TSZ}} = G(\nu)y, \quad \left(\frac{\delta T}{T_0}\right)_{\text{KSZ}} = -\tau \frac{v_{cl}}{c}, \quad (1)$$

where  $G(x) = x \coth(x/2) - 4$ ,  $x = h\nu/k_B T$  is the CMB frequency in dimensionless units,  $v_{cl}$  is the velocity of the cluster projected along the line of sight (*los*) and  $c$  the speed of light. The Comptonization parameter and the optical depth  $\tau$  are defined as

$$y = y_0 \int T_e n_e dl, \quad \tau = \sigma_T \int n_e dl, \quad (2)$$

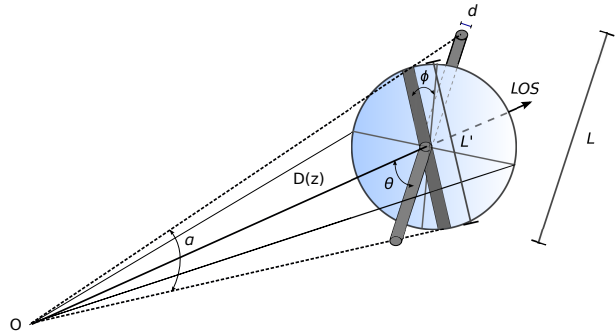


**Figure 1.** Geometrical model of a simple filament with constant density and temperature. The filament has a size  $L$ , width  $d$ , is located at redshift  $z$  at a comoving distance  $D(z)$ , subtends an angle  $\alpha$  from the observer and is randomly oriented in space, forming an angle  $\theta$  with respect to the line of sight.

where  $T_e$  and  $n_e$  are the electron temperature and electron number density,  $dl$  is the proper distance along the *los* and  $y_0 = \sigma_T k_B / m_e c^2$ , with  $\sigma_T$ ,  $k_B$ ,  $m_e$  Thomson cross section, Boltzmann constant and electron mass, respectively. While the KSZ effect has the same frequency dependence as the intrinsic CMB anisotropies, the change with frequency of TSZ effect,  $G(x)$ , is different from that of any other known foreground. It is negative in the Rayleigh-Jeans and positive in the Wien regions, being null close to  $\nu = 217\text{GHz}$  and can be more easily separated from other contributions than KSZ anisotropies. Since they are more easily detectable, here we shall discuss only the TSZ contribution of the WHIM.

An order of magnitude estimate of the WHIM TSZ effect can be obtained by considering the effect on the CMB radiation of a single filament with constant electron density  $n_e$  and constant temperature  $T_e$ . The geometrical configuration of a filament of size  $L$  and thickness  $d$  is shown in Figure 1. For a filament randomly oriented  $\omega \equiv (\theta, \phi)$  in space, let  $\theta$  be the angle between the filament and the *los*. The Comptonization parameter induced in the radiation crossing this filament is

$$y = y_0 \frac{n_e T_e d}{\cos \theta}, \quad (3)$$

where  $d/\cos \theta$  is the projected thickness of the filament. The Comptonization parameter averaged over all possible azimuths  $\phi$  is

$$\langle y \rangle_\phi = y_0 \frac{n_e T_e d}{\cos \theta} \frac{d}{2\pi L}. \quad (4)$$

If the size of filaments at redshift  $z$  is small compared to its angular diameter distance,  $L \ll D_A(z)$ , then the projected comoving length  $L'$  can be written as  $L' = L \cos \theta \sim \alpha D(z)$  where  $D(z)$  is the co-moving distance and  $\alpha$  is the angle subtended by the filament on the sky. Then,

$$\langle y \rangle_\phi = y_0 \frac{n_e T_e L d^2}{2\pi \alpha^2 D^2(z)}. \quad (5)$$

The probability that a given *los* crosses the filament is  $L/(\pi D(z))$ ; if  $d \ll L$ , then the average over all possible values of  $\alpha$  is

$$\langle y \rangle = y_0 \frac{n_e T_e}{2\pi^2} \frac{L}{D(z)} d. \quad (6)$$

In their analysis of the properties of filaments, Klar & Mücke (2012) obtained  $d = \epsilon L$ , with  $\epsilon \in [0.01 - 0.1]$ .

The mean distortion along the *los* can be obtained by adding the effect of all filaments of different masses at different redshifts:

$$\langle y \rangle = \frac{1}{2\pi} \int_z \int_M \frac{dn_f}{dM} dM y_0 n_e T_e \frac{\epsilon L^2(M)}{D(z)} \frac{dV(z)}{dz} dz, \quad (7)$$

where  $n_f$  is the number of filaments per unit of volume. To proceed further we assume that filaments connect clusters and groups of galaxies. Then, their length is approximately the distance between clusters. If  $n_{cl}$  is the number of clusters of a given mass per unit of volume, then the mean separation of the filaments within a volume  $V$  is  $l \sim (V/n_{cl})^{1/3}$  and its mean length  $L \sim n_{cl}^{-1/3}$ . Thus, the mean Comptonization parameter along the *los* is

$$\langle y \rangle = \frac{2}{\pi} \int_z \int_M \frac{dn_f}{dM} dM y_0 n_e T_e \epsilon \frac{D(z)}{n_{cl}(M)^{-2/3}} \frac{dD(z)}{dz} dz, \quad (8)$$

with

$$dD(z) = cH_0^{-1} [\Omega_\Lambda + \Omega_m(1+z)^3 + \Omega_k(1+z)^2]^{1/2} dz, \quad (9)$$

and  $\Omega_k = (1 - \Omega_m - \Omega_\Lambda)$ . Equation (8) can be used to obtain an order of magnitude of the distortion induced by the electrons on the WHIM filaments. If we take  $T_e \approx 10^7$  K,  $\epsilon = 0.05$  and compute the number of filaments according to Sheth & Tormen (2002) then  $y_c = 10^{-6}$ , compatible with the FIRAS upper limit of  $\bar{y}_c = 1.5 \times 10^{-5}$ . The CMB distortion due to a network of filaments of ionized gas is compatible with observations. The integration is performed from  $M_i = 10^{13} M_\odot$  to  $M_f = 10^{15} M_\odot$ . Our results are insensitive to the exact value of  $M_f$  whose number density is exponentially suppressed but depend on  $M_i$  which we took to be the mass of rich groups of galaxies, limit where the number of objects is not longer well described by Sheth & Tormen (2002). Using that formalism Shimon et al. (2012) have calculated the radiation power spectrum. In the next section we will give a more refined prediction based on a log-normal model of the baryon distribution.

### 3 THE LOG-NORMAL BARYON DENSITY DISTRIBUTION MODEL

In perturbation theory, the density contrast is defined as

$$\delta(\mathbf{x}) \equiv \frac{\rho(\mathbf{x}) - \langle \rho \rangle}{\langle \rho \rangle}, \quad (10)$$

where  $\rho(\mathbf{x})$  is the density at any given point and  $\langle \rho \rangle$  the mean density at any given redshift. In Fourier space and in the linear regime, all modes evolve at the same rate and

$$\delta(\mathbf{k}, z) = D_+(z) \delta(\mathbf{k}, 0), \quad (11)$$

where  $D_+(z) = D_+(z, \Omega_\Lambda, \Omega_m)$  is the linear growth factor normalized to  $D_+(0) = 1$ . If the initial density field is a Gaussian random field, then the linearly extrapolated power spectrum  $P(k)$  is defined by

$$\langle \delta(\mathbf{k}, 0) \delta(\mathbf{k}', 0) \rangle = (2\pi)^3 P(\mathbf{k}) \delta(\mathbf{k} - \mathbf{k}'). \quad (12)$$

In eq. 12 the power spectrum  $P(k)$  is that of the background  $\Lambda$ CDM model, computed using linear theory. We took the spectral index at large scales to be  $n_S = 1$ . We did not

consider corrections due to the non-linear evolution of the matter density field on scales about and below  $8h^{-1}$  Mpc.

In the linear regime, baryons follow the Dark Matter (DM) distribution, but this is not longer true once structures become non-linear. In regions where large-scale perturbations develop shocks, Klar & Mücke (2010) showed that the gas perturbations on small scales were suppressed by the enhanced pressure and would be nearly erased. Then, the distribution of the baryon WHIM filaments that are forming and evolving within the large-scale density perturbations would be different from that of the DM. The linear density contrast of baryons in the IGM can be obtained from that of the DM by smoothing over scales below  $L_0$ , the largest scale erased by shock-heating. According to Fang et al. (1993)

$$\delta_B(\mathbf{k}, z) = \frac{\delta_{DM}(\mathbf{k}, z)}{1 + L_0^2 k^2}. \quad (13)$$

The comoving length scale  $L_0$  can be determined by imposing that it is the smallest possible length scale at which the linear peculiar velocity  $v_p$  equals the sound speed  $v_s(z)$  of the baryon fluid. The sound speed is determined by the mean temperature  $T_{IGM}(z)$  of the IGM at any given  $z$ :  $v_s = \sqrt{2k_B T_{IGM}(z)/m_p}$ . The condition  $v_p \geq v_s$  gives

$$L_0(z) = \frac{2\pi(1+z)^2 v_s H_0^{-1}}{(\Omega_\Lambda + \Omega_m(1+z)^3)^{1/2} D_+(z) \delta_0}. \quad (14)$$

In eq. (14), the sound speed is determined by the IGM temperature  $T_{IGM}$  at mean density.  $T_{IGM} \approx 10^4$  K and it is mainly determined by the evolution of the UV background. For that temperature, at redshift  $z = 0$  we have  $L_0 \approx 1.7h^{-1}$  Mpc. This value of cut-off scale agrees with the results of Klar & Mücke (2012) on the formation and evolution of WHIM filaments. Tittley & Meiksin (2007) have studied different ionization models and discussed the possible range of variation of the mean IGM temperature. In our calculations, we assume that  $T_{IGM}$  varies as given in Theuns et al. (2002). Below we shall see that at redshifts  $z > 3$  the WHIM does not generate significant anisotropies. At redshifts  $z \leq 3$ , the mean IGM temperature variation with redshift is small and can be roughly approximated as  $\log_{10}(T_{IGM}/10^3 \text{ K}) \approx (A + 0.1(1+z))$ , where  $A$  varies in the range  $A = 0.5 - 0.9$ , corresponding to  $T_{IGM} = 10^{3.6} - 10^4$  K.

The Fourier transform of eq. (13) gives the density contrast in real co-moving space,  $\delta(\mathbf{x}, z)$ . If the density field grows non-linearly but the velocity field still remains in the linear regime, then the initial Gaussian density field is described by a log-normal density distribution (Coles & Jones 1991). This log-normal model has been shown to describe the matter distribution in hydrodynamical simulations (Bi & Davidsen 1997) and to reproduce the observations of the IGM (Choudhury et al. 2001). For a log-normal density field, the baryon number density is given by

$$n_B(\mathbf{x}, z) = n_0(z) e^{-\Delta_B^2(z)/2} e^{\delta_B(\mathbf{x}, z)} \quad (15)$$

where  $\delta_B$  is the linear baryon density field and  $\Delta_B^2 = \langle \delta_B^2 \rangle$  its variance, with

$$\Delta_B^2(z) = \langle \delta_B^2(\mathbf{x}, z) \rangle = D_+^2(z) \int \frac{P_{DM}(k)}{[1 + k^2 L_0^2]^2} \frac{d^3 k}{(2\pi)^3} \quad (16)$$

If  $\delta_B$  is Gaussian distributed, then the spatial mean  $\langle n_B(\mathbf{x}, z) \rangle$  equals the cosmic baryonic background density  $n_0(z)$ . Hereafter we shall denote by  $\xi = n_B(\mathbf{x}, z)/n_0(z)$  the

non-linear baryon density in units of the baryon mean density.

In Atrio-Barandela & Mücke (2006), Atrio-Barandela et al. (2008) and Génova-Santos et al. (2009) we assumed that the gas in the WHIM follows a polytropic equation of state. High resolution hydro-simulations have shown that at the physical conditions of the WHIM, the shock heated gas at temperatures  $10^5 K < T_e \leq 10^7 K$  and density contrasts  $1 \leq \xi \leq 100$  is not polytropic. Kang et al. (2005) and Cen & Ostriker (2006) provide phase diagrams of electron temperature  $T_e$  versus baryon density  $n_B$  in the range of interest. Since the IGM is highly ionized due photo-ionization by the UV background, then  $n_e \approx n_B$ . This is even more accurate for the WHIM as collisional ionization at high temperatures also contributes to maintain  $n_e = n_B$ . We have used these results to construct fits to the baryon temperature- density distribution,  $T_e = T_e(n_e)$ . We used the fitting formula

$$\log_{10} \left( \frac{T_e(\xi)}{10^8 \text{K}} \right) = -\frac{2}{\log_{10}(4 + \xi^{\alpha+1/\xi})}. \quad (17)$$

This expression fits the results of Kang et al. (2005) when  $\alpha = 1 - 4$ .

The phase space derived from simulations are not simple linear relations of the type  $T_e = T_e(n_e)$ ; phase diagrams have a large scatter. This theoretical uncertainty is important since the Comptonization parameter and temperature anisotropies depend on how steeply the temperature rises with increasing density contrast. We model this uncertainty by taking  $\alpha = 1 - 4$  in eq. (17), a range wide enough to reproduce sufficiently well the phase diagrams and the variation therein. We have also considered the results of Cen & Ostriker (2006); after correcting a possible typo their expression reads  $\log_{10}(T_e/10^8 \text{K}) = -2.5/\log_{10}(4 + \xi)^{0.9}$ . The phase diagrams obtained from cosmological simulations agree qualitatively with the results of Klar & Mücke (2012) on the effect of shocks on WHIM filaments. In particular, as time evolves shocks propagate to lower density regions, steepening the  $T_e - n_e$  relation as shown in the phase diagrams of numerical simulations.

For illustration, in Fig. 2 we plot a series of different fits. The lines with labels  $T_3$  and  $T_4$  correspond to Kang et al. (2005) model with  $\alpha = 1.5$  and 4, respectively,  $T_2$  corresponds to Cen & Ostriker (2006) with the corrected formula given above. For comparison,  $T_1$  corresponds to a simple power law with  $T_e \propto n_e^{3/2}$ . From Fig. 2, we can immediately conclude that since filaments of any density in the  $T_3, T_4$  models are hotter than in the  $T_1, T_2$  models, temperature anisotropies and distortions would be larger in the former than in the latter cases.

#### 4 THE COMPTONIZATION PARAMETER

The log-normal formalism introduced in the previous section permits to compute the statistical properties of the TSZ generated by the baryon population of WHIM filaments. The average Comptonization parameter  $y_{av}$  along a *los* is (Atrio-Barandela & Mücke 2006)

$$y_{av} = y_0 \int \langle n_e(z, x) T_e(z, x) \rangle dl, \quad (18)$$

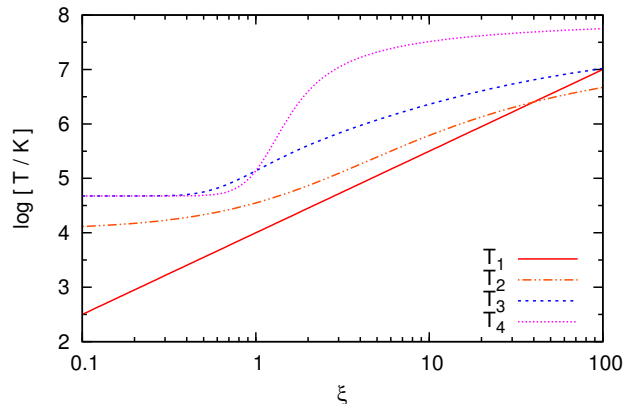


**Figure 2.** Various fit functions  $T_e = T_e(n_e)$  to phase diagrams derived from hydro-numerical simulations. Curves  $T_3, T_4$  correspond to the results of Kang et al. (2004) with  $\alpha = 1.5, 4$ , respectively;  $T_2$  corresponds to Cen & Ostriker (2006); finally,  $T_1$  represents the power law  $T \propto n^{3/2}$ .

where the electron and temperature distribution are given by eqs. (15) and (17), respectively.

The average in eq. (18) must be limited to those scales  $(\xi_1, \xi_2)$  where the non-linear evolution is well described by the log-normal probability density function. The choice of  $\xi_1$  is somewhat arbitrary. Since only gas with density contrasts  $\xi > 2$  will undergo shock-heating, this could be taken as a lower limit. As a criteria, we take  $\xi_1 = \xi_{\text{median}} + \sigma$ , where  $\sigma = \sqrt{\text{var}(\xi)}$  ( $\text{var}(\xi) = \exp(\Delta_B^2) - 1$ ) is the standard deviation of the log-normal distribution. To include only the scales that undergo shocks we also require that  $\xi_1 > 2$  at all redshifts. As upper limit we took  $\xi_2 \leq 100$ , but the results were weakly dependent on this value.

Even though this criteria is somewhat arbitrary, the mass fraction on the interval  $(\xi_1, \xi_2)$  is very close to that of the undetected baryons: 40-50%. At any redshift, the mass fraction of the gas contained in filaments with overdensities in the range  $[\xi_1, \xi_2]$  depends on the IGM temperature. If  $\bar{\xi}$  is the mean of the distribution then  $M(\xi_1, \xi_2) = \bar{\xi}^{-1} \int_{\xi_1}^{\xi_2} \xi F(\xi)$  is the fraction of mass in the integration range. At  $z = 0$ , the fraction of baryons in the WHIM is  $\approx 48\%$  for  $A = 0.9$  and  $\approx 43\%$  for  $A = 0.5$ . One would expect the mass fraction to be largest for  $T_{IGM} = 10^{3.6} \text{K}$ , since smaller scales would survive shock heating than for  $T_{IGM} = 10^4 \text{K}$ . The difference comes from the lower limit  $\xi_1$ . For  $A = 0.5$ , the rms of the log-normal distribution  $\sigma$  is larger and so is  $\xi_1$ ; the integration is carried over a smaller range of densities and low density regions that are included for  $A = 0.9$  are excluded for  $A = 0.5$ . However, even if in this aspect the model is not fully satisfactory, the low dense regions do not contribute significantly to spectral distortions or temperature anisotropies and the exact value of the lower limit  $\xi_1$ , while important for the baryon fraction on the WHIM, has little effect on the final results.

#### 5 THE ANGULAR POWER SPECTRUM

The correlation function of the CMB temperature anisotropies due to the WHIM TSZ contribution along two

different  $l$  and  $l'$  separated by an angle  $\theta$ , is given by (Atrio-Barandela & Mücke 2006)

$$C(\theta) = y_0^2 \int_0^{z_f} \int_0^{z'_f} \langle S(\mathbf{x}, z) S(\mathbf{x}', z') \rangle \frac{dl}{dz} \frac{dl'}{dz'} dz dz', \quad (19)$$

where  $S(\mathbf{x}, z) = n_e(\mathbf{x}, z) T(n_e(\mathbf{x}, z))$ . The density average of eq. (19) is carried out over the same density interval than in eq. (18).

Since the equation of state of the gas is not longer polytropic, the correlation of the electron density at different positions can not be factored out. The average in eq. (19) differs from our previous treatment since now it needs to be computed using the bi-variate log-normal PDF. Remembering that  $\xi = n_B(\mathbf{x}, z)/n_0(z)$ , then

$$\langle S(\mathbf{x}, z) S(\mathbf{x}', z') \rangle = \int \int \xi T(\xi) \xi' T(\xi') F(\xi, \xi') d\xi d\xi', \quad (20)$$

where the bi-variate log-normal PDF  $F(\xi, \xi')$  is given by

$$F(\xi, \xi') = \frac{1}{2\pi \xi \xi' \Delta_B \Delta'_B \sqrt{1-r_c^2}} \exp \left[ -\frac{1}{2(1-r_c^2)} \times \left( \frac{(\log \xi - \mu)^2}{\Delta_B^2} - 2r_c \frac{(\log \xi - \mu)(\log \xi' - \mu')}{\Delta_B \Delta'_B} + \frac{(\log \xi' - \mu')^2}{\Delta_B'^2} \right) \right]. \quad (21)$$

In this expression,  $\Delta_B$  is given by eq. (16),  $\mu = -\Delta_B^2/2$  is the mean of the log-normal PDF and  $r_c$  is the correlation coefficient  $r_c = \langle \log(\xi) \log(\xi') \rangle / (\Delta_B \Delta'_B)$  that in this particular case is given by

$$r_c = \frac{D_+(z) D_+(z')}{2\pi^2 \Delta_B \Delta'_B} \int \frac{P_{DM}(k) j_0(k|\mathbf{x} - \mathbf{x}'|) k^2 dk}{[1 + L_0(z)^2 k^2][1 + L_0(z')^2 k^2]}. \quad (22)$$

In this expression,  $j_0$  denotes the spherical Bessel function of zero order and  $|\mathbf{x} - \mathbf{x}'|$  the proper distance between two patches at positions  $\mathbf{x}(z)$  and  $\mathbf{x}(z')$  separated an angular distance  $\theta$ . In the flat-sky approximation

$$|\mathbf{x} - \mathbf{x}'| \approx \sqrt{l_\perp(\theta, z)^2 + [r(z) - r(z')]^2}, \quad (23)$$

with  $l_\perp(\theta, z)$  the transverse distance of two points located at the same redshift. Therefore, the angular dependence of the correlation function in eq. (19) enters only through eq. (23) in eq. (22).

The power spectrum can be obtained by the Fourier transform of the correlation function (eq. 19)

$$C_\ell = 2\pi \int_{-1}^{+1} C(\theta) P_\ell(\cos(\theta)) d(\cos(\theta)) \quad (24)$$

where  $P_\ell$  denotes the Legendre polynomial of multipoles  $\ell$ .

## 6 RESULTS

To compute the temperature anisotropies generated by the WHIM we take as a background cosmological model the concordance  $\Lambda$ CDM model with densities dark energy, dark matter and baryon fractions  $\Omega_\Lambda = 0.75$ ,  $\Omega_m = 0.25$ ,  $\Omega_b = 0.043$  and Hubble constant  $h = 0.73$  and the amplitude of the matter density perturbations at  $8h^{-1}$ Mpc,  $\sigma_8 = 0.8$ . For simplicity, we fix the frequency dependence of the TSZ effect to unity,  $G(\nu) = 1$ . Our results depend also on physical parameters such as  $L_0$  and the shape of the equation of state. The former is determined by the mean IGM temperature,

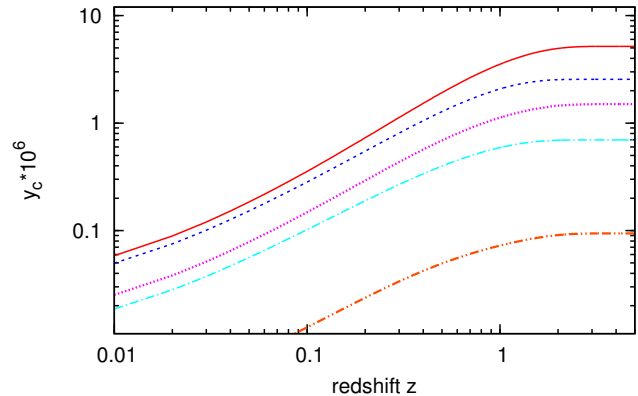


**Figure 3.** Comptonization parameter  $10^6 y$  as a function of redshift. From top to bottom solid and dashed lines corresponds to model  $T_4$  and  $A = 0.5, 0.9$ , dotted and dot-dashed lines to  $T_3$  and  $A = 0.5, 0.9$ , respectively. Finally the double dot-dashed line corresponds to  $T_2$  with  $A = 0.5$ .

characterized by a parameter  $A \approx 0.5 - 0.9$  (see sec. 3) and for the latter we shall consider three different relations: A polytropic equation of state  $T_e \propto n_e^{3/2}$ , the Cen & Ostriker (2006) model and Kang et al (2004) model given by eq. (18) with  $\alpha = 1.5, 4$ , denoted by by  $T_1, T_2, T_3, T_4$ , respectively.

### 6.1 The mean Comptonization parameter

In Fig. 3 we plot the contribution to the average Comptonization parameter  $y_{av}$  from  $z = 0$  up to the given redshift for different models. In all cases, most of the contribution comes from  $z \leq 1$ . In retrospect, this justifies restricting in sec. 3 the IGM temperature parameter to the interval  $A = 0.5 - 0.9$ , valid for the interval  $z \leq 3$ , since baryons at higher redshifts do not contribute to the TSZ effect.

In the figure, the amplitude of the CMB distortion depends on the equation of state and the temperature of the IGM. When  $T_{IGM} = 10^{3.6}$ K smaller (and therefore more) scales contribute to the shock-heated WHIM and  $L_0$  is smaller. Those small scales contribute to the variance of the baryon field at all redshifts (see eq. 16). These regions are of high density and at high temperature and the total effect increases, compensating for the baryon fraction being smaller (see section 4).

### 6.2 The correlation function and the power spectrum

In Fig. 4 we show the power spectrum of the radiation temperature anisotropies generated by the WHIM for different temperature models, obtained by numerical integration of eqs. (19-24). Lines follow the same convention than in Fig. 2. In Fig. 5 we show the dependence with equation of state and  $T_{IGM}$ . The overall shape of the power spectra are very simple: the functional form has a single maximum. For the range of variation of the model parameters, the maximum occurs in the range  $\ell = 200 - 500$  and the maximum amplitude is  $\ell(\ell + 1)C_\ell/2\pi \simeq 0.07 - 70(\mu K)^2$ . The different equations

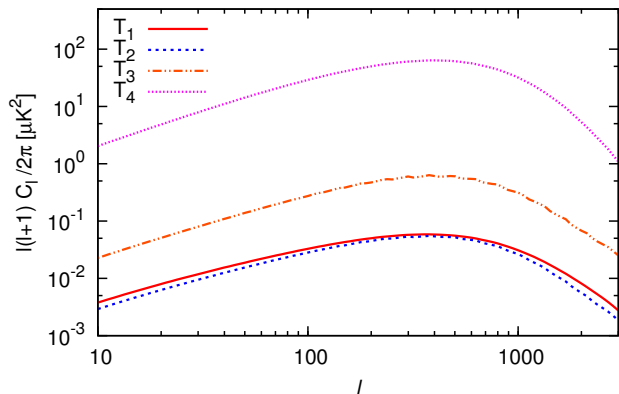


**Figure 4.** Power spectrum of the radiation temperature anisotropies generated by the WHIM. Lines correspond to the models given in Fig.2, with  $A = 0.5$ .

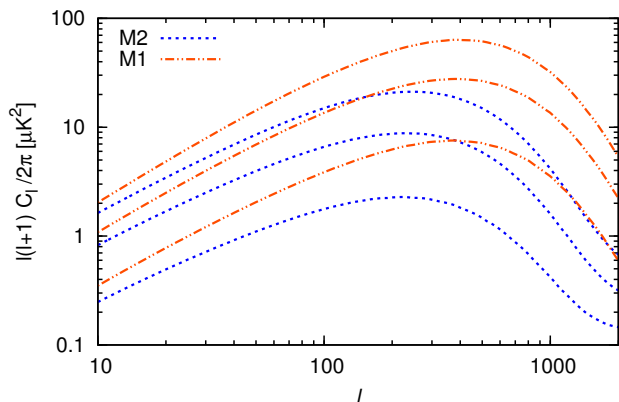


**Figure 5.** Effect of the cut-off length in the radiation power spectra. Curves  $M_1$ ,  $M_2$  correspond to  $A = 0.5$ ,  $A = 0.9$ , respectively. From top to bottom, the equation of state corresponds to the  $T_4$ ,  $T_3$  and  $T_2$  models.

of state  $T_1 - T_4$  give power spectra that differ by three orders of magnitude in amplitude. This wide range reflects our theoretical uncertainty on the equation of state of the shock-heated gas. Using a polytropic equation of state gave even a larger range, and a better determination of the TSZ power spectrum can only come through better understanding of the physics of the WHIM, that is, through cosmological hydro-simulations with larger dynamical range.

The effect of the IGM temperature changes both the amplitude and the location of the maximum. This was to be expected since for smaller IGM temperature the cut-off length  $L_0$  is smaller and the contribution of small scales is more important, increasing the amplitude reducing the average angular size of the anisotropies. For  $A = 0.5$  the power spectrum reaches a maximum at  $\ell \simeq 450$  with an amplitude of  $\ell(\ell+1)C_{\ell,\text{max}}/2\pi \approx 70(\mu\text{K})^2$ . For  $A = 0.9$ , the maximum is at  $\ell \sim 300$  and its amplitude is smaller by a factor  $\sim 3$ .

In Fig. 6 we show the contribution to the power spectrum due to the WHIM at different redshift intervals. Sim-

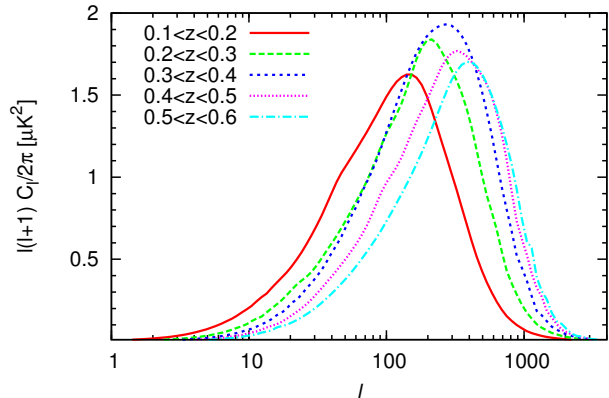


**Figure 6.** Contribution to the power spectrum of different redshift intervals, for the  $T_4$  model with  $A = 0.5$ .

ilarly to what occurs with the Comptonization parameter, the dominant contribution comes  $0.3 < z < 0.5$ , and the contribution for structures with  $z > 1$  is negligible, in agreement with the results of numerical simulations reported by Smith et al. (2011). Again, this justifies the use of a simple parametrization of the IGM temperature that is only valid for redshifts  $z \leq 3$ .

The radiation power spectrum of the WHIM induced temperature anisotropies also depends on the cosmological parameters of the concordance model. As the amplitude of the TSZ effect depends on the number of electrons projected along the  $los$ , the amplitude of the effect scales as  $\Omega_B h$ . Other parameters like  $\Omega_m$  or  $\Omega_\Lambda$  change the induced temperature anisotropies because they change the shape matter power spectrum in eq. (16). But the variance of the linear baryon density field  $\Delta_B^2$  is dominated by the amplitude of the matter power spectrum at small scales, and the largest effect is produced by variations in the amplitude at those scales. Then, the largest variations are produced by changes in  $\sigma_8$ . These are shown in Fig. 7. A linear regression fit to the power spectra of different cosmological parameters gives the following scaling relation at the maximum

$$[(\ell+1)\ell C_\ell]_{\text{max}}/2\pi \propto \sigma_8^{2.6} (\Omega_b h)^2. \quad (25)$$

This scaling relations differ from our previous results in two very important aspects: the power spectrum does not depend so strongly on the model parameters and the TSZ contribution of the WHIM is always smaller than that of clusters. However, like in Atrio-Barandela & Mückel (2006), the bulk of the contribution occurs well within the angular range measured by WMAP and Planck. This opens the possibility of looking for the WHIM contribution in the radiation power spectrum as in Génova-Santos et al (2009). A more suitable data set is the forthcoming Planck data. The high resolution and wide frequency coverage of this instrument makes it feasible to trace the WHIM not only by its power spectrum, but also by the changing amplitude with frequency. In particular, the 217GHz channel, that corresponds to the TSZ null, will help to separate the signal from foreground contributions and other larger systematics.

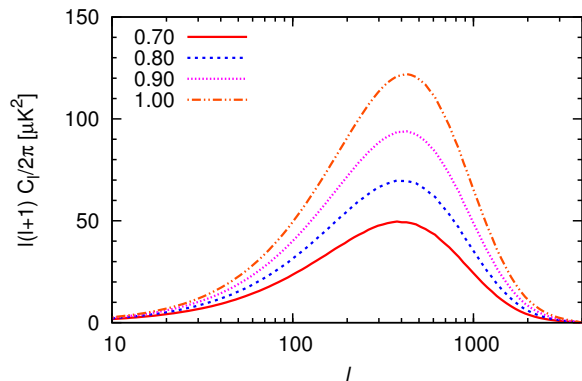


**Figure 7.** Radiation power spectrum for the  $T_4$  model with  $A = 0.5$  and different values of  $\sigma_8$ .

## 7 CONCLUSIONS

We have shown that the gas within non-linear large-scale filaments, with density contrasts  $2 \leq \xi \leq 100$ , shock-heated up to temperatures  $10^5 K < T < 10^7 K$  will produce measurable temperature anisotropies via the TSZ effect. We have assumed that the gas follows the DM distribution that is well described by a log-normal PDF in the density range of interest, in agreement with N-body simulations. The main difference with Atrio-Barandela (2006) and Atrio-Barandela et al (2008) is the adoption of an equation of state  $T_e = T_e(n_e)$ , appropriate to describe the shock-heated gas in the WHIM. The equation of state was derived from phase-diagrams of cosmological hydrodynamical simulations. This complicated the statistical treatment, requiring the statistical averages over densities to be carried out using the bi-variate log-normal PDF. Our final results depend on the cosmological models, the temperature of the IGM and the functional form of the equation of state. We showed that for temperatures compatible with observations and for functional relations derived from numerical simulations, the amplitude of the radiation power spectrum is  $\ell(\ell+1)C_\ell/2\pi = 0.07 - 70(\mu K)^2$ , being its maximum amplitude at  $\ell \simeq 200 - 500$  and with the bulk of the contribution coming from redshift  $z \leq 1.0$ . The large scatter in the final values of the Comptonization parameter and in the amplitude of the power spectra reflects the theoretical uncertainty associated with the functional shape of the temperature-density relation of the shock-heated gas.

The WHIM contribution peaks at a much larger angular scale than  $\ell \sim 3000$ , that of clusters of galaxies, making it accessible to the observations of WMAP and Planck. Recently we have analyzed (Suarez-Velásquez et al. 2012) the observational prospects of the WHIM TSZ by cross-correlating CMB data with tracers of the gas distribution. We concluded that for the current model parameters, the density field reconstructed from the 2MASS galaxy catalog and Planck data could provide the first evidence of the large scale distribution of the WHIM.

## ACKNOWLEDGMENTS

ISV thanks the DAAD for the financial support, grant A/08/73458. FAB acknowledges financial support from the Spanish Ministerio de Educación y Ciencia (grants FIS2009-07238 and CSD 2007-00050). He also thanks the hospitality of the Leibniz-Institut für Astrophysik Potsdam.

## References

- Atrio-Barandela F., Mücke J. P., 2006, *ApJ*, 643, 1  
Atrio-Barandela F., Mücke J. P., Génova-Santos R., 2008, *ApJ*, 674, L61  
Bi H., Davidsen A. F., 1997, *ApJ*, 479, 523  
Cen R., Ostriker J. P., 1999, *ApJ*, 519, L109  
Cen R., Ostriker J. P., 2006, *ApJ*, 650, 560  
Choudhury T. R., Padmanabhan T., Srianand R., 2001, *MNRAS*, 322, 561  
Coles P., Jones B., 1991, *MNRAS*, 248, 1  
Danforth C. W., Shull J. M., 2008, *ApJ*, 679, 194  
Davé R., Cen R., Ostriker J. P., Bryan G. L., Hernquist L., Katz N., Weinberg D. H., Norman M. L., O’Shea B., 2001, *ApJ*, 552, 473  
Davé R., Hernquist L., Katz N., Weinberg D. H., 1999, *ApJ*, 511, 521  
Dietrich J., Werner N., Clowe D. a., 2012, *ArXiv:1207.0809v1*  
Fang L.-Z., Bi H., Xiang S., Boerner G., 1993, *ApJ*, 413, 477  
Fukugita M., Peebles P. J. E., 2004, *ApJ*, 616, 643  
Génova-Santos R., Atrio-Barandela F., Mücke J. P., Klar J. S., 2009, *ApJ*, 700, 447  
Gupta A., Mathur S., Krongold Y., Nicastro F., Galeazzi M., 2012, *ApJ*, 756, L8  
Hallman E. J., O’Shea B. W., Burns J. O., Norman M. L., Harkness R., Wagner R., 2007, *ApJ*, 671, 27  
Kang H., Ryu D., Cen R., Song D., 2005, *ApJ*, 620, 21  
Klar J. S., Mücke J. P., 2010, *A&A*, 522, A114  
Klar J. S., Mücke J. P., 2012, *MNRAS*, 423, 304  
Prochaska J., Tumlinson J., 2008, *ArXiv e-prints*  
Rauch M., 1998, *ARA&A*, 36, 267  
Rauch M., Miralda-Escudé J., Sargent W. L. W., Barlow T. A., Weinberg D. H., Hernquist L., Katz N., Cen R., Ostriker J. P., 1997, *ApJ*, 489, 7  
Richter P., Savage B. D., Sembach K. R., Tripp T. M., 2006, *A&A*, 445, 827  
Schaye J., 2001, *ApJ*, 559, 507  
Shimon M., Sadeh S., Rephaeli Y., 2012, *ApJ*, 10, 38  
Shull J. M., Smith B. D., Danforth C. W., 2011, *ArXiv:1112.2706*  
Smith B. D., Hallman E. J., Shull J. M., O’Shea B. W., 2011, *ApJ*, 731, 6  
Sołtan A. M., 2006, *A&A*, 460, 59  
Stoche J. T., Shull J. M., Penton S. V., 2004, *ArXiv Astrophysics e-prints*  
Suarez-Velásquez I., Kitaura F., Atrio-Barandela F., Mücke J., 2012, *ApJ*, submitted  
Sunyaev R. A., Zeldovich I. B., 1980, *MNRAS*, 190, 413  
Sunyaev R. A., Zeldovich Y. B., 1972, *Comments on Astrophysics and Space Physics*, 4, 173  
Theuns T., Schaye J., Zaroubi S., Kim T.-S., Tzanavaris P., Carswell B., 2002, *ApJ*, 567, L103

Tittley E., Meiksin A., 2007, MNRAS, 380, 1369